



Nitrogen-doped porous carbon coated on graphene sheets as anode materials for Li-ion batteries

Li Su^{1,2} · Lijun Gao^{1,2} · Liyin Hou^{1,2} · Jingmei Li^{1,2} · Wu Yang^{1,2} · Xiujuan Qin^{1,2}

Received: 16 July 2018 / Revised: 20 August 2018 / Accepted: 27 August 2018 / Published online: 20 September 2018
© Springer-Verlag GmbH Germany, part of Springer Nature 2018

Abstract

A hierarchical structure of nitrogen-doped porous carbon coated on graphene sheets (GNC) has been successfully synthesized via a facile method. Notably, nitrogen-doped porous carbon (NC) was prepared by direct calcinations of sodium citrate and urea without aid of any additional carbon source and template. The porous structure arises from the decomposition of sodium citrate and the formative Na_2CO_3 is the hard template during the annealing process. To our pleasure, the 3D architecture is derived from the graphene sheets as skeleton to support porous carbon, which avoids the agglomeration of graphene and enlarges the specific surface area of porous carbon. Besides, using urea as resource of N element promotes a high N-doping level (3.33 atom %) and improves electrical conductivity and lithium storage sites. Thus, the obtained GNC-700 °C as an anode material delivers a high-reversible capacity of 842.7 mAh g^{-1} at 0.1 A g^{-1} and good cycling performances (431.4 mAh g^{-1} at 0.5 A g^{-1} after 200 cycles). The distinguished carbon anode material demonstrates an appealing development for Li-ion batteries.

Keywords N-doped porous carbon · Graphene · Anode material · Li-ion batteries

Introduction

With the crisis of fossil energy resources and serious environmental problems, developing green and sustainable energy storage system with high energy and power densities becomes more and more urgent for modern world [1–7]. Lithium-ion batteries (LIBs), as one of the representative energy storage devices, have been widely devoted to portable electronics owing to their high energy density and long cycling life [8, 9]. As we all know, graphite is the most common but not the most appropriate candidate for anode materials owing to its low theoretical capacity (372 mAh g^{-1}) and poor rate capability

[10–12]. Thus, exploring novel carbon materials with high-specific capacity, high-rate capability, and environmental friendliness is an urgent problem to be solved. Up to now, various carbon-based electrode materials were prepared by typical template method, such as silica template [13, 14], MgO template [15], and NaCl template [16]. However, all of them need additional templates to form specific morphology, which makes process complex. In a word, as an excellent anode material to support outstanding lithium storage performance, it should be not only a large surface area with abundant active sites but also source widely, cost lowly, and preparation simply.

The doping of heteroatoms into carbon, such as nitrogen (N) [17], phosphorus (P) [18], sulfur (S) [19], and boron (B) [20] introduces abundant active sites for lithium storage. Especially, the incorporation of the N element improves the electronic conductivity of the electrode material owing to its five valence electrons for bonding with carbon atoms [21]. More importantly, the doping of the N element promotes electrochemical performance on account of more active sites and increased interaction between carbon and adsorbents [22]. It thus appears that N-rich carbon is an appropriate choice for LIBs anode materials. However, the conductivity and specific surface area of pure porous carbon are difficult to meet the excellent electrochemical energy storage. Graphene, a popular

Li Su and Lijun Gao contributed equally to this work.

Electronic supplementary material The online version of this article (<https://doi.org/10.1007/s11581-018-2713-1>) contains supplementary material, which is available to authorized users.

✉ Xiujuan Qin
qinxj@ysu.edu.cn

¹ Hebei Key Laboratory of Applied Chemistry, College of Environmental and Chemical Engineering, Yanshan University, Qinhuangdao 066004, China

² State Key Laboratory of Metastable Materials Science and Technology, Yanshan University, Qinhuangdao 066004, China

two-dimensional carbon material, has caused great concern for energy conversion and storage because of its well conductivity, large surface area, and mechanical stability [23–25]. Unfortunately, the graphene nanosheets with the p-p stacking interactions tend to aggregate together restricting the migration and storage of Li-ions [26, 27]. Based on the above view, recently, some works are devoted to the combination of graphene and porous carbon to act as an anode material for LIBs. For example, Xie et al. have prepared hierarchical sandwich-like graphene-based N-doped porous carbon through pyrolysis of metal organic frameworks grown on graphene oxide, which shows excellent lithium storage performance [28].

Herein, we construct N-doped porous carbon coated on graphene sheets as anode materials for LIBs. It is noteworthy that NC is prepared via a direct calcination of sodium citrate and urea without of any additional carbon source and template. During the pyrolysis process with the protection of N₂, sodium citrate will be in situ generate hexagonal Na₂CO₃ crystals. And the Na₂CO₃ is the hard template for the formation of porous carbon. Urea, as an ideal resource of N element, promotes a high N-doping level (3.33 atom %). Besides, graphene oxide (GO) is mixed directly to the raw material to form graphene-based N-doped porous carbon during the carbonization process. The 3D architecture is derived from graphene sheets as skeleton to support porous carbon, which avoids the agglomeration of graphene and enlarges the specific surface area of porous carbon. Thus, the sample obtained GNC-700 °C as an anode material delivers a high reversible capacity of 842.7 mAh g⁻¹ at 0.1 A g⁻¹ and good cycling performances (431.4 mAh g⁻¹ at 0.5 A g⁻¹ after 200 cycles). The distinguished electrochemical results demonstrate that the graphene-based N-doped porous carbon is an appealing development as anode material for LIBs.

Experimental section

Synthesis of graphene oxide

Graphene oxide (GO) was prepared from graphite powder by a modified Hummers' method [29, 30]. All the other chemicals are used without further purification.

Synthesis of GNC

Firstly, 0.2 g GO was dissolved into 50 mL deionized water, and then under ultrasonic to form a homogeneous solution. After that, 3.0 g sodium citrate and 0.6 g urea were prepared carefully and added into the above solution, followed by magnetic stirring for 10 min. Finally, put the above solution in an oven at 80 °C for 24 h until dried out. The obtained product was annealed under N₂ atmosphere at temperature (600, 700,

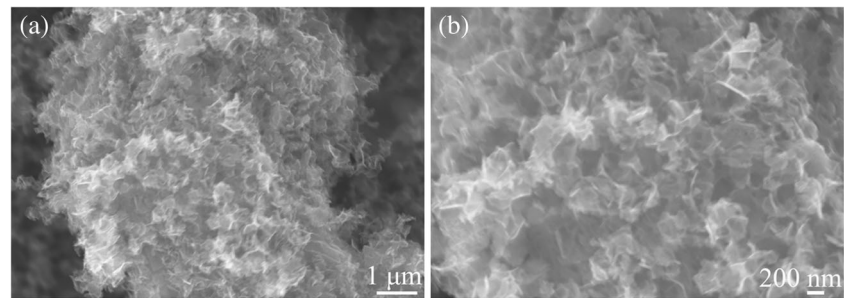
and 800 °C) with a heating rate of 5 °C min⁻¹ for 1 h. The obtained black powder was washed with 1 M HCl to remove impurities and then deionized water to be neutral. The obtained sample was marked GNC-600 °C, GNC-700 °C, GNC-800 °C, respectively. For comparison, pure NC was also prepared by the same method mentioned above except for adding GO, which was marked as NC-700 °C.

Materials characterization

X-ray powder diffraction (XRD, RigakuSmart Lab, X-ray Diffractometer, Japan) was performed to characterize the crystalline structure of the as-prepared products, and XRD data were collected in the range of 5° ≤ 2θ ≤ 60° at a scan rate of 5°/min⁻¹. The Raman spectra was recorded on a Horiva (LabRam HR-800) spectrometer (532 nm, 50 mW excitation laser), and the sample was tested under the Raman laser power of 0.1 mW. The chemical-binding energy of samples was analyzed by X-ray photoelectron spectra (XPS, Thermal ESCALAB 250). In addition, nitrogen adsorption-desorption isotherms tested on a VSorb 2800P analyzer was used to evaluate the surface area and pore structure of the materials using Brunauer-Emmett-Teller (BET) method. Besides, the morphology of the materials was characterized by a field emission-scanning electron microscopy (FE-SEM, Carl Zeiss Super55 operated at 5 kV) and field emission-transmission electron microscope (TEM, Hitachi HT7700 operated at 120 kV), respectively.

Electrochemical measurements

To evaluate the electrochemical performance of the graphene-based N-doped porous carbon material, 2032 coin-type cells were fabricated in a glove box filled with argon, and both water and oxygen levels were below 0.1 PPM. Firstly, the working electrode was prepared by mixing a slurry of active material, polyvinylidene fluoride (PVDF) binder and acetylene black with a weight ratio of 7:2:1 in the N-methyl-2-pyrrolidone (NMP) solvent, and then uniformly deposited onto a smooth copper foil followed by drying in a vacuum oven at 110 °C for 12 h to remove the NMP solvent away. Finally, the dried material was cut into electrodes with a diameter of 1 cm. The mass loading of the electrode was approximately 1.6 mg cm⁻² and the loading weight of the active material was 1.0 ~ 1.2 mg cm⁻². Besides, lithium foil was used as the counter and reference electrode. 1 M LiPF₆ dissolved in a mixture of ethylene carbonate (EC) and diethyl carbonate (DEC) with a volume ratio of 1:1 was as electrolyte. The galvanostatic charge-discharge testing was performed at a LAND-CT2001A battery testing system (Wuhan, China). The cyclic voltammetry (CV) was tested by CHI 660E (Shanghai, China) electrochemical workstation, which performed at a scan rate of 0.1 mV S⁻¹ within the voltage of 0.01–3.0 V (vs. Li⁺/Li).

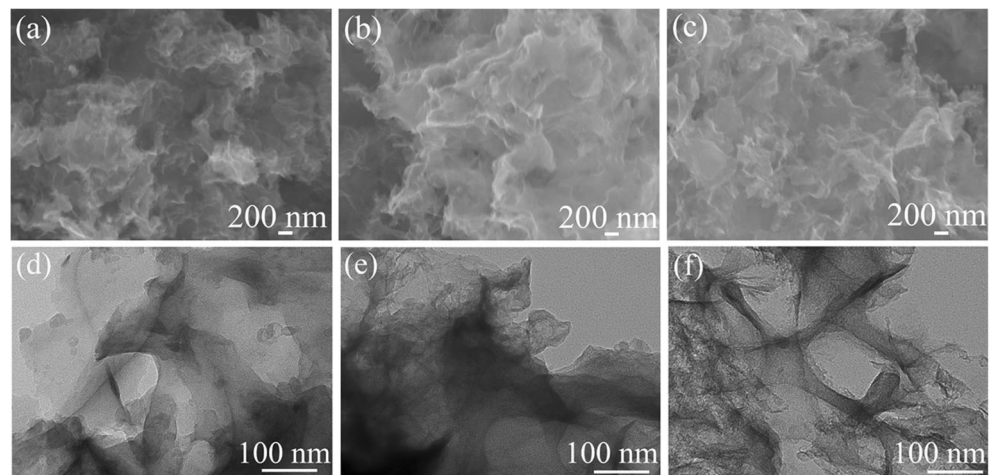
Fig. 1 SEM images of NC-700 °C

Results and discussions

To investigate the morphology of the obtained samples, SEM and TEM studies are employed. Firstly, the TEM image of pure GO is presented in Fig. S1, which suggests that the GO has been separated into two-dimensional layered structure with wrinkles. The SEM images of precursors are shown in Fig. S2. As seen in Fig. S2a, the material obtained by just mixing sodium citrate and urea presents thick and independent bulks. However, with the addition of GO, the precursor turns to be laminar and coherent (Fig. S2b). Owing to the oxidation stripping of GO, there are many functional groups (–COOH, –OH, etc.) on its surface, then basing on the electrostatic force between each other, sodium citrate and urea can be a good combination on the surface of graphene, and graphene as a skeleton to show the lamellar structure. Figure 1 shows SEM images of NC-700 °C. It can be seen that NC-700 °C is made up of many nanoscale carbon plates connected together to form a porous 3D structure. Besides, there are many mesoporous on the surface, which contributes to the electrolyte wetting and accommodates the structure change during charge-discharge process. The 3D porous carbon structure is caused by forming the $\text{Na}_2\text{CO}_3@\text{C}$ during high-temperature heat treatment of sodium citrate. Here, these Na_2CO_3 crystals act as hard template for the growth of network-like product during subsequent carbonization process. After washing by HCl solution and deionized water, Na_2CO_3 was removed and 3D

porous carbon network structure was obtained. Moreover, Fig. 2a–f shows SEM and TEM of GNC under different carbonization temperatures (GNC-600 °C, GNC-700 °C, and GNC-800 °C). Satisfactorily, the morphologies of all GNC products display thin and loose layers with wrinkles as shown in Fig. 2a–c, and we can also see that graphene is well combined with porous carbon. The design of a smart 3D architecture will avoid the agglomeration of graphene and enlarges the specific surface area of porous carbon. However, there are slight changes on the three products with the rise of carbonization temperature. When the temperature is 800 °C, the structure turns to be loose and the laminar structure is not obvious because of the damage of high temperature. In this way, 700 °C is the most appropriate temperature for remaining the most integrated and cross-linked porous structure. As displayed in Fig. 2d–f, there are obvious porous heterostructures and these properties conduct to the wetting of electrolyte and shorten the diffusion pathway of Li-ions, which can be beneficial to the storage of Li-ions.

XRD patterns of the obtained samples are presented in Fig. 3a. Firstly, we can see that the XRD of NC-700 °C shows two broad peaks located at 23.6° and 43.6°, which can be assigned to the (002) and (100) reflections of carbon, respectively. It reveals the characteristic of amorphous carbon obviously. Besides, we can see that all of the three GNC samples also display two obvious characteristic peaks. However, the peaks of GNC samples are obviously sharper than those of NC-700 °C, which attributes to the addition of GO and makes

Fig. 2 SEM images of GNC-600 °C (a), GNC-700 °C (b), GNC-800 °C (c), and TEM images of GNC-600 °C (d), GNC-700 °C (e), and GNC-800 °C (f)

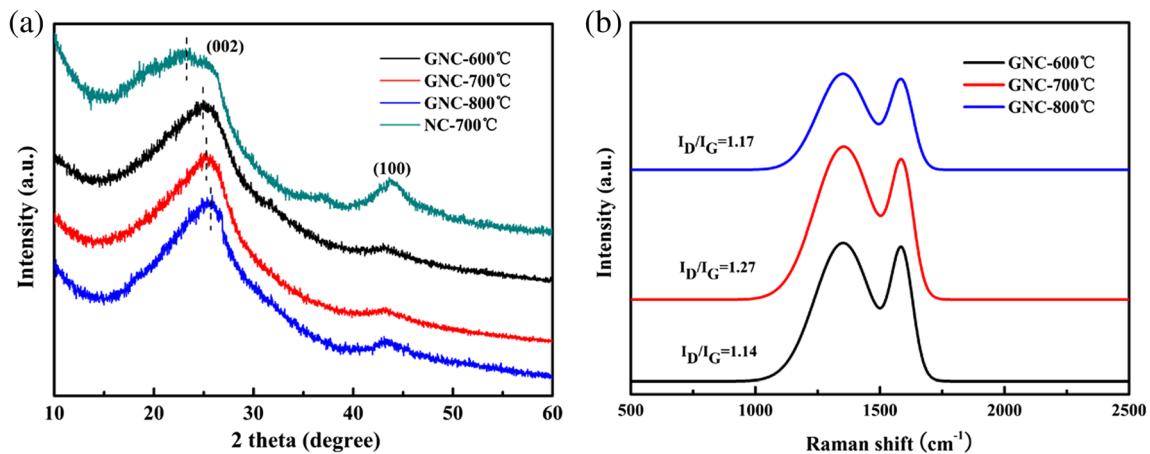
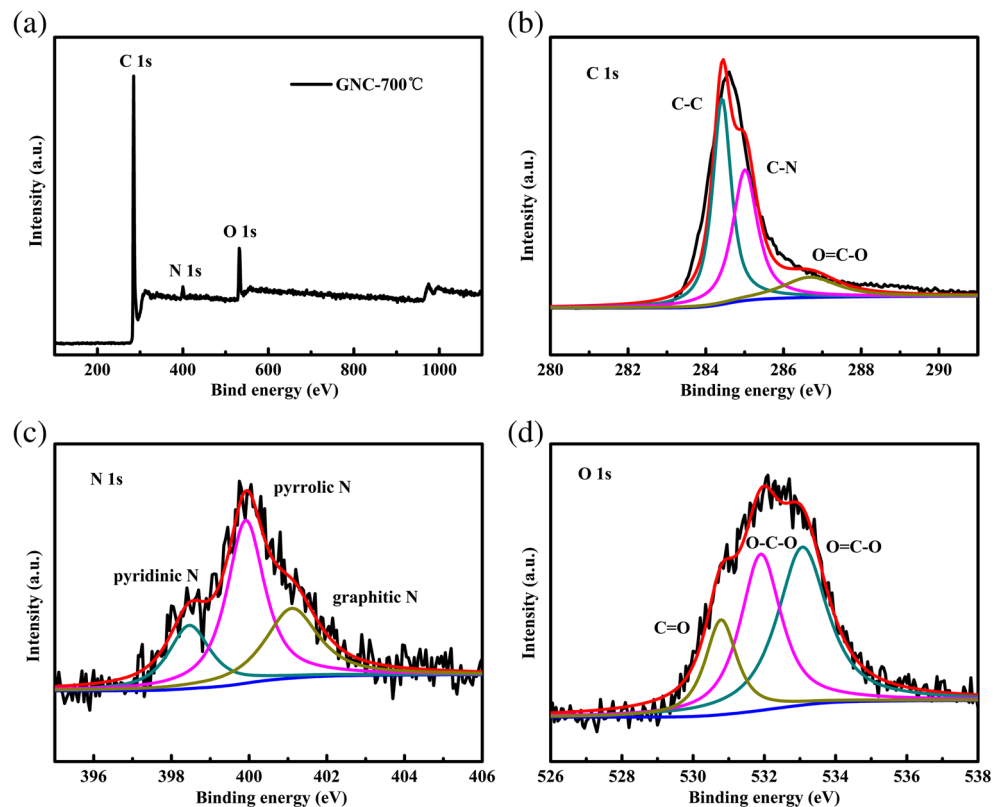


Fig. 3 XRD patterns of NC-700 °C, GNC-600 °C, GNC-700 °C, and GNC-800 °C (a), and Raman spectra of GNC-600 °C, GNC-700 °C, and GNC-800 °C (b)

the increase of graphitization. Furthermore, the electric conductivity measured under 7 MPa of NC-700 °C and GNC-700 °C is 0.66 and 2.74 S cm⁻¹, respectively, indicating that the addition of graphene could improve the electrochemical conductivity of the composite. Moreover, in comparison to GNC-600 °C, the (002) peaks of GNC-700 °C and GNC-800 °C obviously shift to the higher angle, which specifies an enlarger degree of order with the carbonization temperature increasing. Raman spectroscopy is also a powerful evidence for analyzing the structure changes of carbon materials. The Raman spectrum of three samples reveals two typical peaks at

1590 cm⁻¹ and 1350 cm⁻¹ (Fig. 3b), corresponding to G band and D band, respectively. Generally speaking, G band reflects the degree of graphitization and D band represents the defect of carbon materials. The intensity ratios of I_D/I_G of three samples are 1.14, 1.27, and 1.17, respectively, which indicates relative high defects and disorders for GNC-700 °C. That may result from the porous structure and structural distortion induced by nitrogen doping. For N-doped carbon as anode materials, the lithium storage properties largely rely on the doped nitrogen type and amount. Thus, XPS was performed on the GNC-700 °C to analyze the elemental composition and

Fig. 4 XPS survey spectrum of GNC-700 °C (a), C 1s XPS spectra of GNC-700 °C (b), N 1s XPS spectra of GNC-700 °C (c), and O 1s XPS spectra of GNC-700 °C (d)



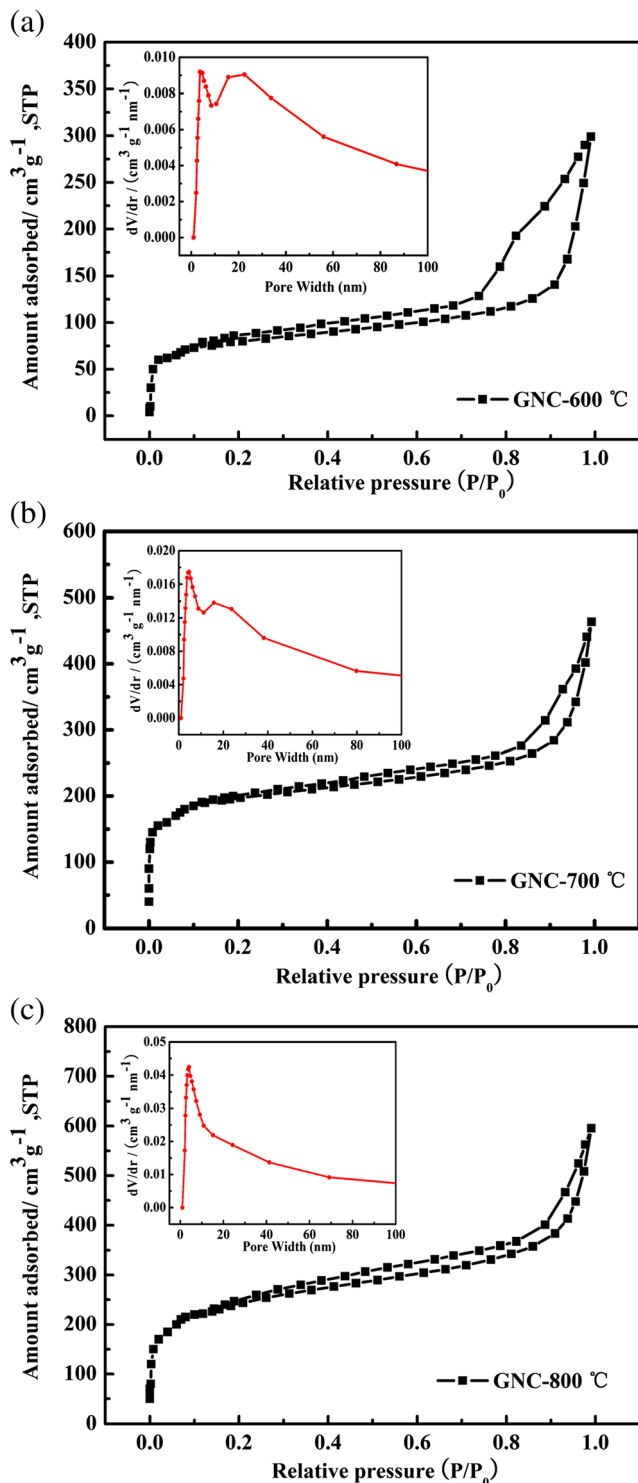


Fig. 5 Nitrogen adsorption-desorption isotherm and pore size distribution of GNC-600 °C (a), GNC-700 °C (b), and GNC-800 °C (c)

amount. The XPS survey spectrum of GNC-700 °C (Fig. 4a) possesses three peaks located at 285 eV, 400 eV, and 532 eV, corresponding to C 1 s, N 1 s, and O 1 s, respectively. Besides, the contents of the three elements are 87.58 atom%, 3.33 atom%, and 9.09 atom%, respectively. The XPS spectrum of C

1 s (Fig. 4b) can be divided into three peaks. The main peaks at 284.7 eV, 285.2 eV, and 287.1 eV correspond to C–C, C–N, and O=C–O groups, respectively [31, 32]. Figure 4c shows the N 1 s spectrum, it can be divided into three main peaks located at 398.5 eV, 399.6 eV, and 400.8 eV. As most reports demonstrate, it indicates the existence of pyridinic, pyrrolic, and graphitic nitrogen, respectively, which corresponds to common combining ways in N-doping porous carbon [17, 33, 34]. On the one hand, the doping of nitrogen atom modifies the surface properties of carbon materials, which is beneficial to the wetting of electrolyte [35]. On the other hand, it increases the conductivity of carbon materials and the active sites of Li-ion storage. Meanwhile, XPS spectrum of O 1 s is shown in Fig. 4d. Three peaks located at 531.2 eV, 532.3 eV, and 533.5 eV indicates C=O, O–C–O, and O=C–O, respectively. The oxygen mainly comes from the thermostable oxygen-containing components of the carbon materials, as well as a little water and oxygen from the surface of the materials. To analyze the specific surface area and pore size distribution of the carbon materials, Fig. 5 supplies nitrogen adsorption-desorption isotherm and pore size distribution of GNC-600 °C, GNC-700 °C, and GNC-800 °C. Obviously, three samples present a similar typical type-IV curve suggesting that there are a large number of mesopores. The inset of Fig. 5 is corresponding to pore size distribution, and the BET surface area and porosity parameters of the synthesized materials are presented in Table 1. With the rise of carbonization temperature, the gradually increased BET surface areas of GNC are 293.6, 743.5, and 873.1 m² g⁻¹, respectively. The larger surface area of GNC-700 °C and GNC-800 °C is conducive to expand the contact area between electrolyte and electrode and active sites for Li-ion storage, which improves high-specific capacity and good rate capability. The total pore volume increases from 0.38 to 0.68 cm³ g⁻¹ with the increase of carbonization temperature. That may attribute to a more efficient activation process during high-temperature carbonization, which forms more pores in the carbon materials. Besides, the average pore diameter of the three samples is 6.30, 3.85, and 4.22 nm, respectively, which shows mesopore concentrated at approximately 3–7 nm.

To evaluate lithium storage properties of the as-prepared bare NC and GNC samples, various electrochemical measurements are performed. Figure 6a presents cyclic voltammetry curves of GNC-700 °C at a scan rate of 0.1 mV s⁻¹ between 0.01 and 3.0 V vs Li/Li⁺. Obviously, it is a kind of typical curve of N-doped porous carbon anode materials [36, 37]. During the first cycle, a sharp reduction peak appears around 0.6 V, which dues to the formation of the solid electrolyte interphase (SEI) and some secondary reactions. In the subsequent cycles, the sharp peak disappears and all CV curves are almost overlapped, which implies the formation of a stable SEI layer after the first cycle and the good reversibility of electrode material. During the anodic scanning process, the oxidation peak around 0 V is attributed to the removal of Li-

Table 1 BET surface area and porosity parameters of GNC-600 °C, GNC-700 °C, and GNC-800 °C

Sample	BET surface area [m ² g ⁻¹]	Total pore volume [cm ³ g ⁻¹]	Average pore diameter [nm]
GNC-600 °C	293.6	0.38	6.30
GNC-700 °C	743.5	0.48	3.85
GNC-800 °C	873.1	0.68	4.22

ions from the graphite layer and the oxidation peak around 1.2 V exists because Li-ion takes off from the defect of electrode materials, which are consistent with the anode reaction mechanism: $\text{Li}_x\text{C}_6 \rightarrow \text{C} + x \text{Li}^+ + x \text{e}^-$ [38]. Figure 6b show charge–discharge profiles of GNC-700 °C at the current density of 0.1 A g⁻¹. The first discharge capacity of GNC-700 °C is 1639.1 mAh g⁻¹ and the reversible charge capacity is 803.6 mAh g⁻¹. It can thus be concluded that the initial coulombic efficiency is 49.0%. The large irreversible capacity loss attributes to the formation of a solid-electrolyte interphase (SEI) film that matches well with the CV results [39]. Due to the carbon material that features large specific surface area, the poor initial coulombic efficiency commonly occurs in carbon-based anodes. Rate-capability behaviors of GNC-600 °C, GNC-700 °C, and GNC-800 °C at various specific currents

are shown in Fig. 6c. The GNC-700 °C electrode shows a reversible capacity of 842.7 mAh g⁻¹, 731.6 mAh g⁻¹, 579.2 mAh g⁻¹, 455.3 mAh g⁻¹, 375.4 mAh g⁻¹, and 258.5 mAh g⁻¹ at the current density of 0.1, 0.2, 0.5, 1, 2, and 5 A g⁻¹, respectively. When the rate is reduced back to 0.1 A g⁻¹ after cycling at above current density, the capacity can still be recovered to 836.8 mAh g⁻¹ implying a good reversibility for the material. However, the GNC-600 °C and GNC-800 °C anodes show much lower reversible capacities of 601.2 and 542 mAh g⁻¹, 523.9 and 440.4 mAh g⁻¹, 432.8 and 327.2 mAh g⁻¹, 355.1 and 239.4 mAh g⁻¹, 318.2 and 200 mAh g⁻¹, and 230.5 and 133.4 mAh g⁻¹ when performed at 0.1, 0.2, 0.5, 1, 2, and 5 A g⁻¹, respectively. The good rate capability of GNC-700 °C electrode is ascribed to its smart design in which graphene sheets act as a skeleton to support

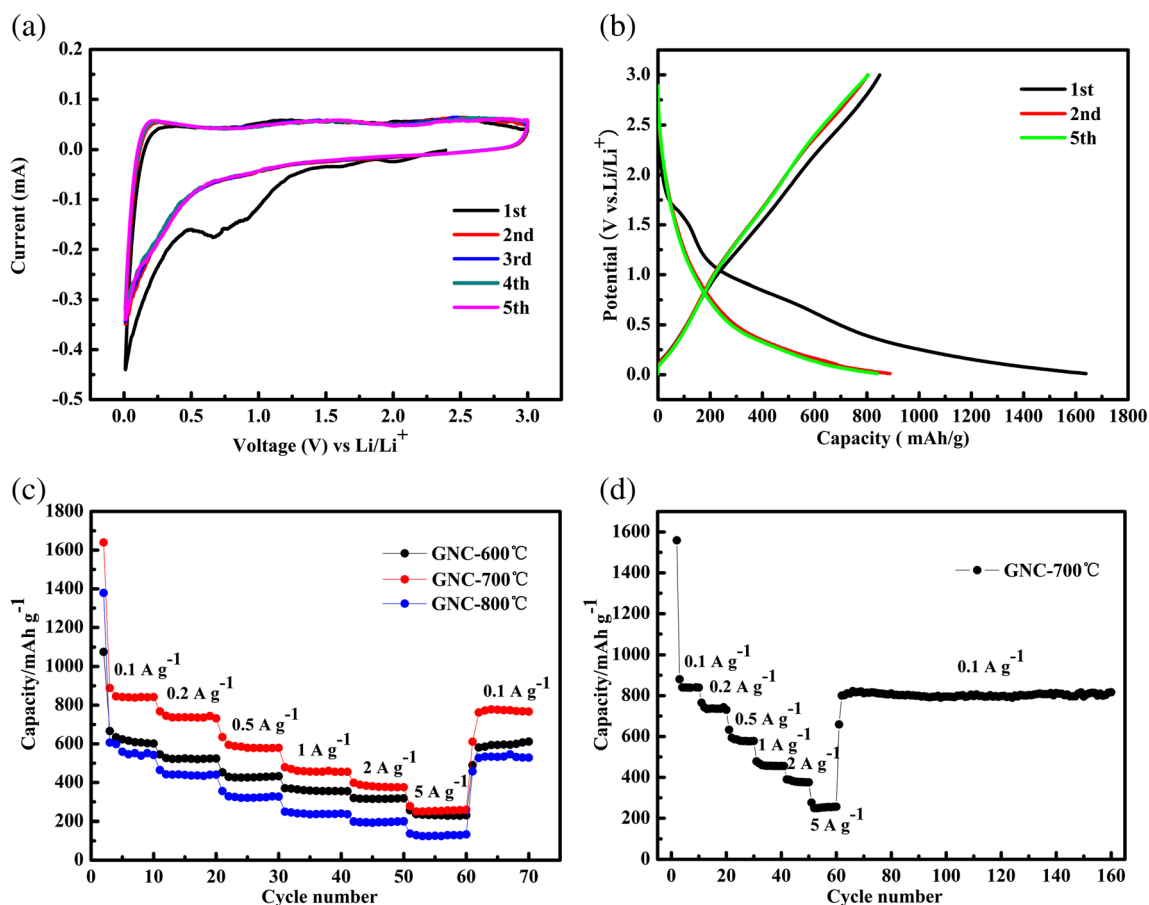


Fig. 6 Cyclic voltammetry curves of GNC-700 °C at a scan rate of 0.1 mV s⁻¹ (a), charge–discharge profiles of GNC-700 °C at 0.1 A g⁻¹ (b), rate capability of GNC-600 °C, GNC-700 °C, and GNC-800 °C at various specific currents (c), and rate capability and cycling test of GNC-700 °C (d)

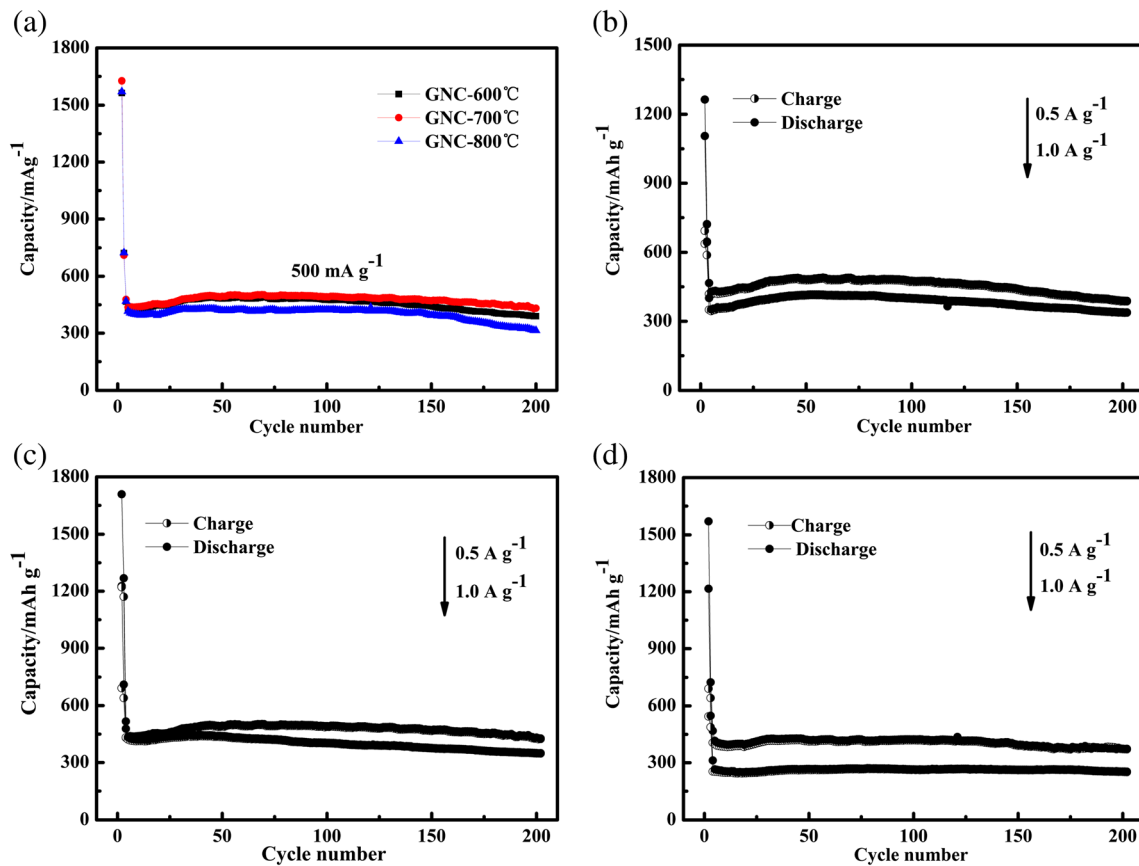


Fig. 7 Cycling test of GNC-600 °C, GNC-700 °C, and GNC-800 °C at 0.5 A g⁻¹ (a), GNC-600 °C at 0.5 A g⁻¹ and 1 A g⁻¹ (b), GNC-700 °C at 0.5 A g⁻¹ and 1 A g⁻¹ (c), and GNC-800 °C at 0.5 A g⁻¹ and 1 A g⁻¹ (d)

porous carbon, which avoids the agglomeration of graphene and enlarges the specific surface area of porous carbon. Meanwhile, sufficient defects are obtained for GNC-700 °C by high N doping, which is beneficial to increase the active sites of the lithium storage. It is worth mentioning that although GNC-800 °C is with a large specific surface area it is likely to lower N content of the material when the temperature is relatively high, which reduces the defects of materials and causes low-lithium storage capacity. As shown in Fig. 6d, after rate capability tests for 60 cycles, GNC-700 °C electrode was performed at the current density of 0.1 A g⁻¹ for 100 times and specific capacity can remain 816.5 mAh g⁻¹ indicating the good cycle performance of GNC-700 °C electrode material. In addition, in order to evaluate the effect of graphene, cycling test at 0.5 A g⁻¹ and 1 A g⁻¹ for NC-700 °C, and GNC-700 °C is shown in Fig. S3. It can be seen that a significant improvement of reversible capacity and outstanding stability for GNC-700 °C. Besides, long cycle tests at 0.5 A g⁻¹ for GNC samples with different temperatures are also displayed in Fig. 7a. We can see that three samples show similar but slightly different curves after 200 cycles. Obviously, the specific capacities of all GNC samples increase in the first few dozen cycles, which attributes to the delayed wetting of the electrolyte into electrode along with the gradual activation process. After full

wetting, we realize that the discharge capacity of the GNC electrode declines gradually in the following cycles, which may be because Li atoms irreversibly bind in the vicinity of H atoms in these hydrogen-containing carbons [40]. To see the contrast more clearly, the cycling test of each material at both 0.5 A g⁻¹ and 1 A g⁻¹ is also present in Fig. 7b–d. Undoubtedly, GNC-700 °C owns better capacity performance, which contributes to its high-N content and large specific surface area. It is noted that the electrochemical performance of GNC-700 °C exceeds most carbon-based works reported in recent years, and corresponding comparison table is shown in Table S1.

Electrochemical impedance spectroscopy (EIS) is an effective approach to evaluate the performance for LIBs. As shown in Fig. 8, the Nyquist plots of the three electrodes consist of a semicircle at a high-frequency region and an oblique Warburg line in the low-frequency range. As we all know, the semicircle in the high-frequency region represents the charge transfer impedance (R_{ct}), whereas the sloped line in the low-frequency region stands for the Warburg impedance. It can be seen that the charge transfer resistances of GNC-700 °C are smaller than that of the GNC-600 °C and GNC-800 °C, which means better electrochemical kinetics. Meanwhile, the GNC-700 °C shows a more vertical line than GNC-600 °C and GNC-

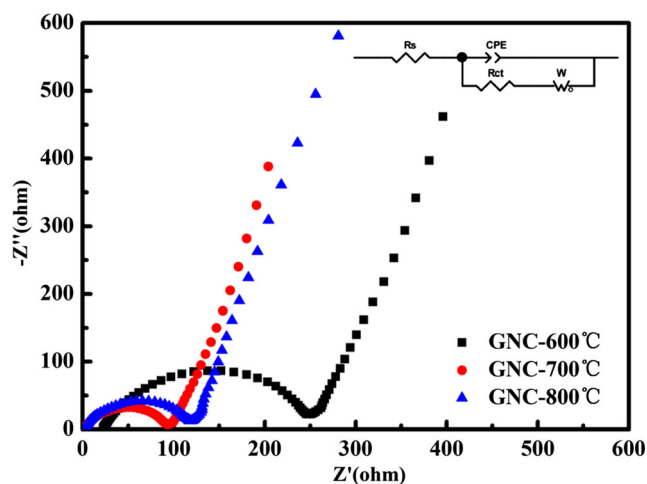


Fig. 8 Nyquist plots of GNC-600 °C, GNC-700 °C, and GNC-800 °C

800 °C implying the lower diffusion resistance. Besides, we calculate corresponding kinetic parameters of GNC-600 °C, GNC-700 °C, and GNC-800 °C. As shown in Table 2, the values of R_s and R_{ct} for the GNC-700 °C electrode are 2.09 and 92.4 Ω , respectively, which are lower than those of GNC-600 °C electrode (22.3 and 234.8 Ω) and the GNC-800 °C electrode (2.49 and 121.2 Ω). Meanwhile, exchange current density (I_0) is an effective criterion for evaluating electrochemical properties of electrode materials according to the equation $I_0 = RT/nFR_{ct}$ [41]. The value of the exchange-current density I_0 for GNC-700 °C is the highest (1.67 mA cm^{-2}) of the three electrodes, indicating well electrochemical activity of GNC-700 °C with respect to lithium storage. According to the above EIS results, it is reasonable to believe that the unique 3D hierarchical nanostructure of N-doped porous carbon coated on graphene sheets is responsible for the excellent electrochemical performance for LIBs.

Conclusions

In summary, a hierarchical structure of N-doped porous carbon coated on graphene sheets has been successfully synthesized via a facile method with direct calcination of sodium citrate and GO without aid of any additional template. The outstanding electrochemical properties as carbon-based

Table 2 Kinetic parameters of GNC-600 °C, GNC-700 °C, and GNC-800 °C

Sample	$R_s(\Omega)$	$R_{ct}(\Omega)$	$I_0(\text{mA cm}^{-2})$
GNC-600 °C	22.3	234.8	0.66
GNC-700 °C	2.09	92.4	1.67
GNC-800 °C	2.49	121.2	1.27

Note: the exchange current density I_0 was calculated according to the equation of $I_0 = RT/nFR_{ct}$

anodes for LIBs were demonstrated, and the superior energy-storage performance of GNC anodes may benefit from the following: (i) The 3D architecture is derived from graphene sheets as a skeleton to support porous carbon, which avoids the agglomeration of graphene and enlarges the specific surface area of porous carbon. (ii) The successful realization of porous structure mainly arises from the decomposition of sodium citrate, which releases a large amount of CO_2 gases during the annealing process. (iii) Urea acts as N resource to promote a high N-doping level (3.33 atom %) for improving electrical conductivity and active sites for lithium storage. As a consequence, GNC with rational porous structure and N-doping level demonstrates to be a significant alternative to commercial graphite anode in high-performance LIBs.

Funding information This research received financial support from the Natural Science Foundation of Hebei Province (B2018203330).

References

- Wang F, Wu X, Li C, Zhu Y, Fu L, Wu Y, Liu X (2016) Nanostructured positive electrode materials for post-lithium ion batteries. *Energy Environ Sci* 9:3570–3611
- Kim H, Kim H, Ding Z, Lee MH, Lim K, Yoon G, Kang K (2016) Recent progress in electrode materials for sodium-ion batteries. *Adv Energy Mater* 6:1600943
- He Y, Chen W, Li X, Zhang Z, Fu J, Zhao C, Xie E (2013) Freestanding three-dimensional graphene/MnO₂ composite networks as ultralight and flexible supercapacitor electrodes. *ACS Nano* 7:174–182
- Su L, Gao L, Du Q, Hou L, Ma Z, Qin X, Shao G (2018) Construction of NiCo₂O₄@MnO₂ nanosheet arrays for high-performance supercapacitor: highly cross-linked porous heterostructure and worthy electrochemical double-layer capacitance contribution. *J Alloys Compd* 749:900–908
- Liu W, Li X, Xiong D, Hao Y, Li J, Kou H, Yan B, Li D, Lu S, Koo A, Adair K, Sun X (2018) Significantly improving cycling performance of cathodes in lithium ion batteries: the effect of Al₂O₃ and LiAlO₂ coatings on LiNi_{0.6}Co_{0.2}Mn_{0.2}O₂. *Nano Energy* 44:111–120
- Jin R, Li X, Sun Y, Shan H, Fan L, Li D, Sun X (2018) Metal-organic frameworks-derived Co₂P@N-C@rGO with dual protection layers for improved sodium storage. *ACS Appl Mater Interfaces* 10:14641–14648
- Fan L, Li X, Song X, Hu N, Xiong D, Koo A, Sun X (2018) Promising dual-doped graphene aerogel/SnS₂ nanocrystal building high performance sodium ion batteries. *ACS Appl Mater Interfaces* 10:2637–2648
- Tarascon JM (2010) Is lithium the new gold? *Nat Chem* 2:510
- Sun G, Yin X, Yang W, Zhang J, Du Q, Ma Z, Shao G, Wang Z (2018) Synergistic effects of ion doping and surface-modifying for lithium transition-metal oxide: synthesis and characterization of La₂O₃-modified LiNi_{1/3}Co_{1/3}Mn_{1/3}O₂. *Electrochim Acta*
- Xu W, Xie Z, Cui X, Zhao K, Zhang L, Mai L, Wang Y (2016) Direct growth of an economic green energy storage material: a monocrySTALLINE jarosite-KFe₃(SO₄)₂(OH)₆-nanoplates@rGO hybrid as a superior lithium-ion battery cathode. *J Mater Chem A* 4:3735–3742
- Nishihara H, Kyotani T (2012) Energy storage: templated nanocarbons for energy storage (*Adv. Mater.* 33/2012). *Adv Mater* 24:4466–4466

12. Kaskhedikar NA, Maier J (2010) Lithium storage in carbon nanostructures. *Adv Mater* 21:2664–2680
13. Li D, Ding LX, Chen H, Wang S, Li Z, Zhu M, Wang H (2014) Novel nitrogen-rich porous carbon spheres as a high-performance anode material for lithium-ion batteries. *J Mater Chem A* 2:16617–16622
14. Guo DC, Han F, Lu AH (2015) Porous carbon anodes for a high capacity lithium-ion battery obtained by incorporating silica into benzoxazine during polymerization. *Chem* 21:1520–1525
15. Zhu C, Akiyama T (2016) Cotton derived porous carbon via an MgO template method for high performance lithium ion battery anodes. *Green Chem* 18:2106–2114
16. Lu P, Sun Y, Xiang H, Liang X, Yu Y (2018) 3D amorphous carbon with controlled porous and disordered structures as a high-rate anode material for sodium-ion batteries. *Adv Energy Mater* 8
17. Li Z, Xu Z, Tan X, Wang H, Holt CMB, Stephenson T, Olsen BC, Mitlin D (2013) Mesoporous nitrogen-rich carbons derived from protein for ultra-high capacity battery anodes and supercapacitors. *Energy Environ Sci* 6:871–878
18. Wu Y, Fang S, Jiang Y (1998) Carbon anode materials based on melamine resin. *J Mater Chem* 8:2223–2227
19. Chen L, Song L, Zhang Y, Wang P, Xiao Z, Guo YG, Cao F (2016) Nitrogen and sulfur co-doped reduced graphene oxide as a general platform for rapid and sensitive fluorescent detection of biological species. *ACS Appl Mater Interaces* 8:11255
20. Yin G, Gao Y, Shi P, Cheng X, Aramata A (2003) The effect of boron doping on lithium intercalation performance of boron-doped carbon materials. *Mater Chem Phys* 80:94–101
21. Hou J, Cao C, Idrees F, Ma X (2015) Hierarchical porous nitrogen-doped carbon nanosheets derived from silk for ultrahigh-capacity battery anodes and supercapacitors. *ACS Nano* 9:2556–2564
22. Shin WH, Jeong HM, Kim BG, Kang JK, Choi JW (2012) Nitrogen-doped multiwall carbon nanotubes for lithium storage with extremely high capacity. *Nano Lett* 12:2283–2288
23. Li J, Lu L, Kang T, Cheng S (2016) Intense charge transfer surface based on graphene and thymine–Hg (II)–thymine base pairs for detection of Hg²⁺. *Biosens Bioelectron* 77:740–745
24. Eda G, Lin YY, Mattevi C, Yamaguchi H, Chen HA, Chen IS, Chen CW, Chhowalla M (2010) Blue photoluminescence from chemically derived graphene oxide. *Adv Mater* 22:505–509
25. Zhu D, Wang L, Xu X, Wei J (2016) Label-free and enzyme-free detection of transcription factors with graphene oxide fluorescence switch-based multifunctional G-quadruplex-hairpin probe. *Biosens Bioelectron* 75:155–116
26. Chen Y, Zhang X, Yu P, Ma Y (2009) Stable dispersions of graphene and highly conducting graphene films: a new approach to creating colloids of graphene monolayers. *Chem Commun* 30:4527
27. Mukherjee R, Thomas AV, Krishnamurthy A, Koratkar N (2012) Photothermally reduced graphene as high-power anodes for lithium-ion batteries. *ACS Nano* 6:7867–7878
28. Xie Z, He Z, Feng X, Xu W, Cui X, Zhang J, Yan C, Carreon MA, Liu Z, Wang Y (2016) Hierarchical sandwich-like structure of ultrafine N-rich porous carbon nanospheres grown on graphene sheets as superior lithium-ion battery anodes. *ACS Appl Mater Interaces* 8:10324–10333
29. Jr WSH, Offeman RE (1958) Preparation of graphitic oxide. *J Am Chem Soc* 80:1339
30. Ai W, Zhou W, Du Z, Du Y, Zhang H, Jia X, Xie L, Yi M, Yu T, Huang W (2012) Benzoxazole and benzimidazole heterocycle-grafted graphene for high-performance supercapacitor electrodes. *J Mater Chem* 22:23439–23446
31. Qian W, Sun F, Xu Y, Qiu L, Liu C, Wang S, Yan F (2013) Human hair-derived carbon flakes for electrochemical supercapacitors. *Energy Environ Sci* 7:379–386
32. Jang JW, Lee KS, Lyu SC, Lee TJ, Lee CJ (2004) Structural study of nitrogen-doping effects in bamboo-shaped multiwalled carbon nanotubes. *Appl Phys Lett* 84:2877–2879
33. Wei D, Liu Y, Wang Y, Zhang H, Huang L, Yu G (2009) Synthesis of N-doped graphene by chemical vapor deposition and its electrical properties. *Nano Lett* 9:1752–1758
34. Palaniselvam T, Biswal BP, Banerjee R, Kurungot S (2013) Zeolitic imidazolate framework (ZIF)-derived, hollow-core, nitrogen-doped carbon nanostructures for oxygen-reduction reactions in PEFCs. *Chem* 19:9335–9342
35. Zhao J, Lai H, Lyu Z, Jiang Y, Xie K, Wang X, Wu Q, Yang L, Jin Z, Ma Y (2015) Hydrophilic hierarchical nitrogen-doped carbon nanocages for ultrahigh supercapacitive performance. *Adv Mater* 27:3541–3545
36. Mao Y, Duan H, Xu B, Zhang L, Hu Y, Zhao C, Wang Z, Chen L, Yang Y (2012) Lithium storage in nitrogen-rich mesoporous carbon materials. *Energy Environ Sci* 5:7950–7955
37. Yang W, Yang W, Kong L, Song A, Qin X, Shao G (2017) Phosphorus-doped 3D hierarchical porous carbon for high-performance supercapacitors: a balanced strategy for pore structure and chemical composition. *Carbon*
38. Wang Z, Huang X, Chen L (1999) Lithium insertion/extraction in pyrolyzed phenolic resin. *J Power Sources* 81–82:328–334
39. Yang W, Yang W, Song A, Sun G, Shao G (2018) 3D interconnected porous carbon nanosheets/carbon nanotubes as a polysulfide reservoir for high performance lithium-sulfur batteries. *Nanoscale* 10:816–824
40. Dahn JR, Zheng T, Liu Y, Xue JS (1995) Mechanisms for lithium insertion in carbonaceous materials. *Science* 270:590–593
41. Zhou X, Chen F, Bai T, Long B, Liao Q, Ren Y, Yang J (2016) Interconnected highly graphitic carbon nanosheets derived from wheat stalk as high performance anode materials for lithium ion batteries. *Green Chem* 18:2078–2088